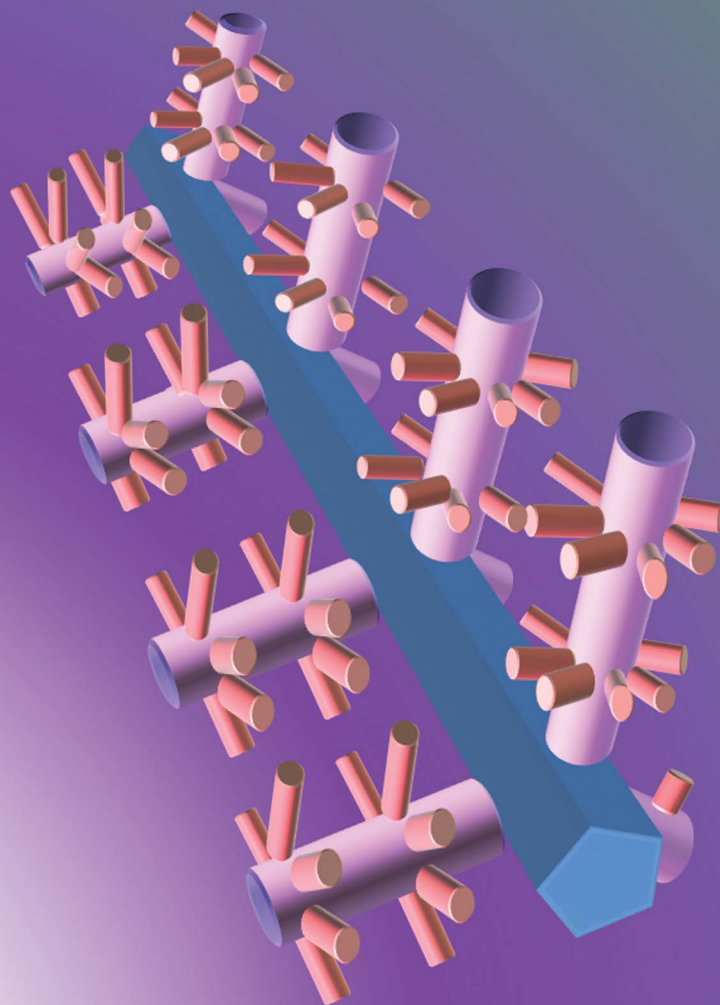


# Nanoscale

www.rsc.org/nanoscale

Volume 4 | Number 19 | 28 September 2012 | Pages 5763–6074



ISSN 2040-3364

RSC Publishing

**COVER ARTICLE**

Yang *et al.*

Synthesis and photocatalysis of hierarchical heteroassemblies of ZnO branched nanorod arrays on Ag core nanowires



**NCNST**



2040-3364 (2012) 4:19;1-C

Cite this: *Nanoscale*, 2012, **4**, 5895

www.rsc.org/nanoscale

PAPER

# Synthesis and photocatalysis of hierarchical heteroassemblies of ZnO branched nanorod arrays on Ag core nanowires†

Shaowu Wang,<sup>a</sup> Yang Yu,<sup>a</sup> Yuanhui Zuo,<sup>b</sup> Chunzhong Li,<sup>c</sup> Jinhu Yang<sup>\*bc</sup> and Conghua Lu<sup>\*a</sup>

Received 28th May 2012, Accepted 24th June 2012

DOI: 10.1039/c2nr31316b

In this paper, hierarchical heteroassemblies made of interwoven Ag core nanowires (NWs) covered by ZnO branched nanorods (ZnO BNRs) are successfully prepared on a large scale *via* a solution bottom-up strategy coupling with a templating method. Briefly, heteroepitaxial growth of ZnO nanorods (ZnO NRs) on ZnO seed-coated Ag NWs is first conducted to form fluffy worm-like heteroassemblies. Then, by templating these, ZnO BNRs with exposed high-energy (001) planes on Ag NWs are fabricated with preserved morphology through the second nucleation and growth processes. When evaluated with UV-induced photo-degradation of rhodamine B (RhB), the heteroassemblies of Ag NWs–ZnO BNRs exhibit high photocatalytic properties, due to the decisive roles of the synergistic effect of the unique metal–semiconductor heterojunction and the hierarchical fluffy worm-like morphologies as well as the (001) plane-dominant surface of ZnO BNRs which are attractive for highly efficient photocatalysis.

## 1. Introduction

Recently, metal–semiconductor nanoheterostructures have attracted increasing interest because these hybrid materials exhibit unique advanced optical, electrical, magnetic and catalytic properties, which endow them with novel unprecedented functions or enhanced performances.<sup>1–4</sup> To date, a variety of metal–semiconductor nanocomposites with complex structures and dimensions have been prepared such as the delicate combination of Au–CdS,<sup>1</sup> Au–PdS,<sup>5</sup> Au–CdSe,<sup>6</sup> Hg–β-HgS<sup>3</sup> and metal–Ag<sub>2</sub>S.<sup>4</sup> Among the metal–semiconductor hybrids, Ag–ZnO hierarchical structures have drawn special attention<sup>2,7–13</sup> due to their superior physical/chemical properties and wide applications in the fields related to solar-energy conversion,<sup>12</sup> microelectronics<sup>13</sup> and especially, photocatalysis.<sup>8–11</sup>

Roughly speaking, there are three kinds of Ag–ZnO nano-hybrids that have been prepared so far, and investigated basically with photocatalysis for organic pollutant degradation. They include Ag–ZnO composite nanoparticle (NP),<sup>10,11</sup> Ag

NP–ZnO nanorod (NR)<sup>2,7,8</sup> and ZnO NR–Ag nanowire (NW)<sup>9</sup> hybrids. It is generally admitted that effective separation and fast transfer of an electron–hole pair on a Ag–ZnO interface driven by UV irradiation are two key factors in determining the catalytic activity of the materials. However, they are highly dependent on the Ag–ZnO heterostructures which are closely related to not only physical properties of materials but also catalytic kinetics of reactions. From the viewpoint of photocatalysis, the above-mentioned Ag–ZnO hybrid structures with isolated ZnO or Ag particles,<sup>2,7,8,10,11</sup> or sparse ZnO NRs<sup>9</sup> with relatively inert side planes exposed, are either not conducive to direct and fast electron transfer or not active enough to prompt the proceeding of photocatalytic reactions, which inevitably lead to drawbacks to the overall efficiency more or less. In fact, as a noble metal with high electrical conductivity and good resistance to corrosion,<sup>14–17</sup> Ag nanowires (NWs) have been applied in a wide variety of devices such as robust flexible electronics<sup>13</sup> and mesh transparent electrodes.<sup>12,18</sup> On the other hand, one-dimensional (1D) structured semiconductors have been well known for their unique characteristics of high accessible specific surface<sup>19a</sup> and relatively high electron mobility,<sup>19b</sup> making them attractive for solar cells,<sup>20</sup> gas sensors<sup>21</sup> as well as photocatalysis.<sup>22</sup> Hopefully, incorporation of a 1D building block of ZnO and Ag NWs into integrated heterogeneous nanostructures is of great significance to obtain superior photoelectric properties of highly efficient separation and transfer of photoinduced charges. In addition, the Ag–ZnO heterostructures reported previously were often realized on a small scale and *via* site-specific recognition between the (001) plane of ZnO and the (111) plane of Ag due to their small structure mismatch (2.68%). However, for the purpose of practical applications, controllable large-scale synthesis of a

<sup>a</sup>School of Materials Science and Engineering, Tianjin University, Tianjin 300072, China. E-mail: chlu@tju.edu.cn

<sup>b</sup>Department of Chemistry, Institute for Advanced Materials and Nano Biomedicine, Tongji University, Shanghai 200092, China. E-mail: yangjinhu2010@gmail.com

<sup>c</sup>Key Laboratory for Ultrafine Materials of Ministry of Education, School of Materials Science and Engineering, East China University of Science and Technology, Shanghai 200237, China

† Electronic supplementary information (ESI) available: synthesis of Ag nanowires and ZnO seeds; synthesis and characterization of ZnO nanosheets and CdS nanotube arrays on Ag nanowires; synthesis of ZnO nanorod and nanosheet arrays on coverslips; SEM images of ZnO nanorod arrays on Ag nanowires at different growth times and different concentrations. See DOI: 10.1039/c2nr31316b

Ag–ZnO hybrid with favored structures for photocatalysis, without the limitation of specific crystal plane recognition, is highly desired.

Therefore, taking all of this into account, we demonstrate here the large-scale synthesis of Ag–ZnO hierarchical hetero-assemblies made of Ag NWs covered with dense ZnO NRs, and then based on these we fabricate morphology-preserved assemblies of Ag NWs–ZnO BNRs with exposed active (001) planes. Such heteroassemblies consisting of 1D building blocks are good candidates for photocatalysis due to their structural advantages: 1D Ag or ZnO nanoblocks for high rate electron/hole transfer, accessible large surface area for effective molecule adsorption/desorption, exposed high-energy (001) planes (ZnO) for active catalyzation and branched structures for efficiently light trapping. On the other hand, these hierarchical assemblies deposited on arbitrary substrates have additional advantages of convenient separation and recycling over the traditional photocatalysts which are in the form of NPs. To the best of our knowledge, the novel nanoheterostructures of Ag NWs–ZnO BNRs are reported here for the first time. As expected, the typical Ag–ZnO nanoheteroassemblies displayed high photocatalytic activities in RhB photodegradation. Moreover, photocatalytic mechanisms involving the influence of key factors such as charge separation, crystal plane energy as well as diffusion kinetics induced by the heterostructures on photocatalysis, have been discussed briefly.

## 2. Experimental section

### 2.1 Synthesis of Ag NW–ZnO NR heteroassemblies

Ag NWs with the aspect ratio of  $\sim 100$  were synthesized by the reduction of silver nitrate in the presence of poly(vinylpyrrolidone) (PVP) ( $M_w = 30\,000$ ) in ethylene glycol (EG) according to the references (S1, ESI $\dagger$ ).<sup>14</sup> Then, the obtained Ag NWs were dispersed in the prepared ZnO seed solution (S2, ESI $\dagger$ ).<sup>32</sup> After 40 min stirring, the suspension was centrifuged at 2500 rpm followed by washing with ethanol twice. Subsequently, the obtained ZnO seed-coated Ag NW suspension was cast onto a cleaned substrate of a glass slide. After the full evaporation of ethanol, the substrate covered with a uniform coating of ZnO seed-coated Ag NWs was dried at 60 °C for 1 h to promote a strong adhesion of Ag NWs to the substrate. Then, the substrate was suspended upside down in a 30 mL aqueous solution composed of equimolar zinc nitrate (0.05 M) and hexamethylenetetramine (HMT) (0.05 M). After incubation at 95 °C for 6 h, the substrate was removed from the solution, rinsed thoroughly with deionized water, and dried in the air.

### 2.2 Synthesis of Ag NW–ZnO BNR heteroassemblies

0.306 mL of 0.1 M sodium citrate solution was added to 30 mL of the above ZnO NR growth solution containing equimolar zinc nitrate (0.05 M) and HMT (0.05 M). Then, the as-prepared ZnO NR-grown Ag NWs were immersed and incubated at 95 °C for 1 h. As a result, the ZnO NRs were evolved into the branched NRs.

### 2.3 Characterization

The products were analyzed by a scanning electron microscope (SEM, Hitachi S-4800) with an energy-dispersive spectrometer

(EDAX Genesis XM2) attached. Transmission electron microscopy (TEM) was recorded on a JEOL 100CX-II transmission electron microscope and a FEI Technai G2 F20 high-resolution transmission electron microscope (HRTEM) coupled with an energy-dispersive X-ray spectrometer (EDX). X-ray diffraction (XRD) patterns were obtained on a Rigaku D/max 2500v/pc diffractometer. Optical microscopy images were taken from an inverted Observer A1 microscope (Zeiss, Germany) equipped with a charge-coupled device camera. UV-vis spectroscopy was carried out on a T6 NEW CENTURY spectrophotometer.

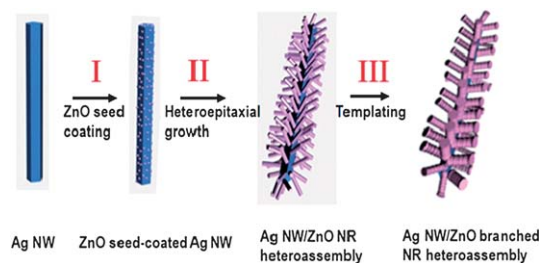
### 2.4 Photocatalytic activity measurement

The ( $2 \times 2$  cm<sup>2</sup>) coverslips covered with the as-prepared Ag NW-based nanostructures upside were immersed in 10 mL rhodamine B (RhB) aqueous solution ( $5\text{ mg L}^{-1}$ ) and kept in dark for 1 h to ensure an adsorption/desorption equilibrium. Then they were irradiated by a 400 W high-pressure Hg lamp with the wavelength range of 350–450 nm while the dominate wavelength was 365 nm (95 cm away from the RhB aqueous solution). After every 30 min UV exposure, the samples were taken out from the RhB solution and then the UV-vis spectrum of the corresponding solution was measured. The UV-induced degradation of RhB in the solution was estimated with the optical density change of RhB at 554 nm.

## 3. Results and discussion

Controlled synthesis of hierarchical Ag NW-based assemblies by a simple solution bottom-up strategy has been illustrated in Scheme 1. Firstly, Ag NWs were coated with ZnO seeds *via* a surface adsorption process (Scheme 1, I). Then a uniform mesh film composed of interlaced ZnO seed-coated Ag NWs was formed on a substrate, followed by the growth of ZnO NRs on the surface of Ag NWs (Scheme 1, II) to form hierarchical heteroassemblies. Furthermore, the as-prepared Ag NW–ZnO NR assemblies were used as the template for morphology-preserved synthesis of ZnO BNR assemblies on Ag core NWs *via* secondary nucleation and growth procedures (Scheme 1, III).

According to the typical solution method reported by Sun and Xia (S1, ESI $\dagger$ ),<sup>14</sup> we synthesized high-quality Ag NWs of 150–180 nm in diameter and 10–15  $\mu\text{m}$  in length (Fig. 1a). Obviously the Ag NWs are organized in an orderly manner on the substrate due to the uniform one-dimensional morphology and the surface-capped functional poly(vinylpyrrolidone) (PVP).<sup>23</sup> In the following step, PVP acts as a polydentate ligand of metal cations



**Scheme 1** A schematic illustration of the procedure for the controllable synthesis of the hierarchical nanostructures of Ag NW-based assemblies *via* the aqueous solution approach.

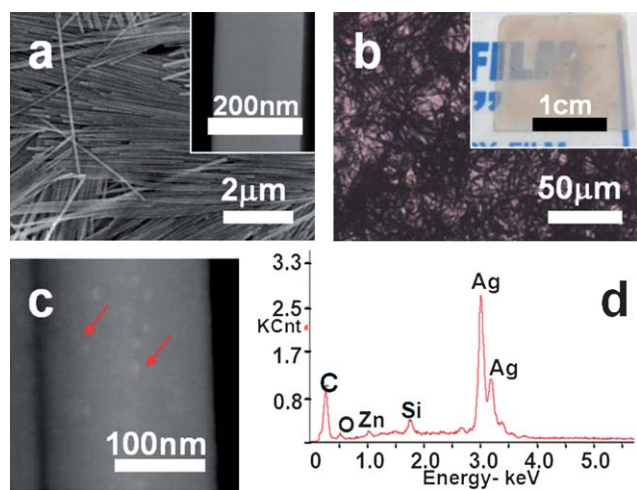


**Fig. 1** SEM (a and c) and optical microscopy (b) images of the as-prepared Ag NWs (a) and the film composed of interwoven ZnO seed-coated Ag NWs (b and c). Panel (d) is the recorded EDAX pattern of the ZnO seed-coated Ag NWs shown in (c). Insets in (a) and (b) show the corresponding high-magnification SEM image and low-magnification CCD image, respectively.

to promote the surface adsorption of ZnO seeds. After being deposited on the substrate, the ZnO seed-coated Ag NWs are intertangled to form a uniform semitransparent mesh film over the area of the substrate, as shown in the low magnification digital photograph (Fig. 1b, inset). Compared with the pristine clean Ag NWs (Fig. 1a, inset), the surface of the resultant ZnO seed-adsorbed Ag NWs is decorated with 3–5 nm-sized NPs, as denoted by the arrows in Fig. 1c. The corresponding EDAX pattern proves the adsorption of ZnO seeds on the surface of Ag NWs (Fig. 1d). This is an essential and crucial step for preparation of Ag–ZnO heteroassemblies with dense ZnO NR covering in large amounts.

Fig. 2 shows the typical structures of Ag NW-based dense ZnO NR assemblies. It is found that ZnO NRs are almost vertically grown on the whole surface including the tips of Ag NWs, forming hierarchical fluffy worm-like structures (Fig. 2a and b). Generally, the assembled ZnO NRs are 1–1.2 μm in length and ~100 nm in diameter, estimated from the close view of the magnified SEM image (Fig. 2b, inset). Here X-ray diffraction (XRD) analysis is employed to investigate the crystal structure of the ZnO NR-grown Ag NWs (Fig. 2c, upper curve). For comparison, the XRD result for the Ag NWs has also been provided (Fig. 2c, bottom curve). Obviously, the synthesized Ag NWs are indexed to the face-centered cubic phase of pure Ag with the intense (111) diffraction peak (JCPDS, No.04-783), in good agreement with the reported result.<sup>14</sup> In the case of ZnO NR-grown Ag NWs, the diffraction peaks, except those indexed to Ag NWs marked with red stars, are well assigned to the wurtzite ZnO (JCPDS, No.36-1451). The decrease in the intensity of the (111) diffraction peaks of Ag results from densely grown ZnO NRs on the surface. The existence of the strongest (002) diffraction peak suggests the assembled ZnO NR arrays on Ag NWs have the [001] preferential orientation. These hierarchical nanostructures can be further verified with the recorded TEM images (Fig. 2d and f). It is noted that the sample with

relatively small diameter of ZnO rods prepared at a low nutrient concentration (0.01 M) is selected for TEM characterization. The low-magnification TEM image clearly shows that ZnO NRs are radially grown on the observable backbone of the Ag NWs (Fig. 2d). The HRTEM image of one ZnO NR shows the lattice spacing of 0.26 nm (Fig. 2f), which corresponds to the (002) plane of ZnO. This indicates that single-crystalline ZnO NRs grown on the Ag NWs have the typical [001] growth direction, resulting in the strongest (001) diffraction peak in the recorded XRD pattern (Fig. 2c). According to crystal symmetry of the wurtzite ZnO, these NRs with [001] growth direction are generally enclosed by relatively inert planes of  $\pm(100)$  as the side surfaces, compared with the high energy of the (002) top plane.

The incubation time-dependent morphology evolution has been studied with SEM (Fig. S1†). It indicates that the hierarchical structures of ZnO NR-grown Ag NWs have the similar growth process as the familiar ZnO NR arrays grown on planar substrates.<sup>24</sup> Here, the film composed of interwoven Ag NWs just acts as the non-planar substrate and the adsorbed ZnO seeds on Ag NWs play a dominant role in the formation of the above hierarchical assemblies. For example, ZnO NRs are selectively grown on the ZnO seed-coated Ag NWs, rather than on the naked substrate, as marked by the arrows shown in Fig. 3a and b. Contrarily, when the pristine Ag NWs without ZnO seeds adsorbed on their surface were utilized under the same conditions, sparse ZnO NRs with a disordered orientation and a larger diameter (~500 nm) are preferentially deposited on the substrate, other than on the Ag NWs (Fig. 3c). These results exclude the influence of the specific crystal-plane recognition between Ag core NWs and subsequently grown ZnO NRs.<sup>2</sup>

On the other hand, the length and diameter of ZnO NRs can be tuned well by the concentration of the nutrient solution (Fig. S2†). When the concentration of equimolar Zn(NO<sub>3</sub>)<sub>2</sub> and HMT varies from 0.01, to 0.025 and 0.1 M, the length of dense ZnO NRs almost remains at ~1.2 μm, while the diameter increases from 40, to 75 and 200 nm, respectively. Meanwhile, the orientation of ZnO NRs on Ag NWs is increasingly improved, which has been well explained in the previous references of ZnO NR arrays on planar substrates.<sup>25</sup>

It has been reported that the highly polar (or high-energy) (001) plane of ZnO crystals is more photoelectrically active than other non-polar planes such as (100) planes.<sup>26,27</sup> Since citrate has been used as an effective agent to induce ZnO platelet generation with top/bottom faces bounded by  $\pm(001)$  planes,<sup>24</sup> the as-prepared Ag NW-based ZnO NRs are incubated in the citrate-contained growth solution to produce ZnO nanostructures with the desirable (001) plane orientation, *via* new nucleation and the secondary growth on the “substrate” of ZnO NRs. As a result, the resultant hierarchical assemblies with ZnO branched NRs are generated (Fig. 4), which differ markedly from the primary ZnO NR-grown Ag NWs (Fig. 2). The XRD pattern demonstrates that the novel nanostructures of ZnO are still the hexagonal wurtzite structure (Fig. 4c). Compared with the parent ZnO NR-grown Ag NWs (Fig. 2c), the intensity of (100) and (101) diffraction peaks in the recorded XRD pattern of Ag NW–ZnO branched NR assemblies has been greatly enhanced (Fig. 4c). Seemingly, the branched NRs deposited on the surface of Ag NWs are composed of stacked nanoplates (Fig. 4b and d). However, the HRTEM images of a sonicated sample clearly

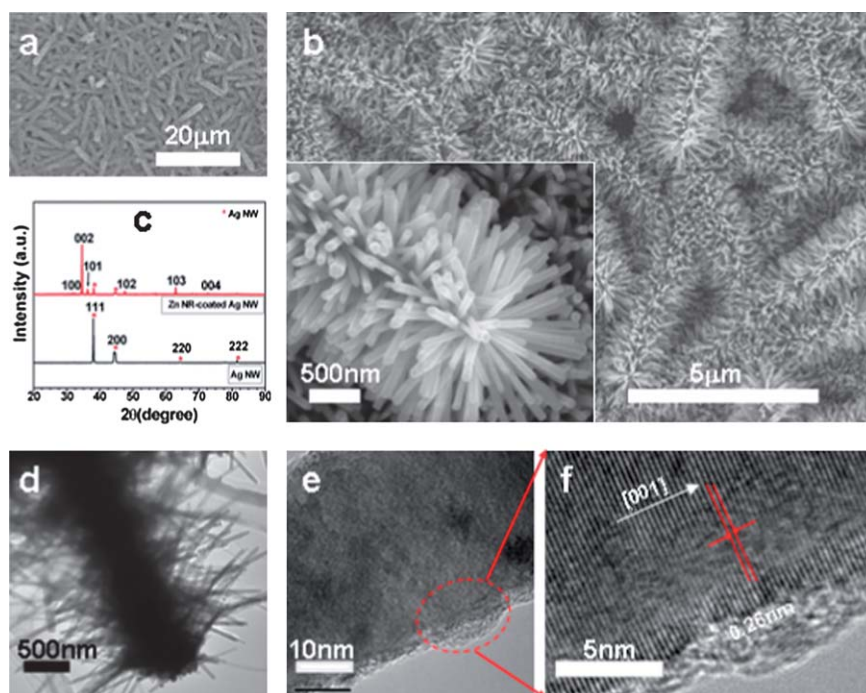


**Fig. 2** SEM (a and b), TEM (d) and HRTEM (e and f) images of the as-prepared hierarchical nanostructures of ZnO NR-grown Ag NWs from 0.05 M (a–c) and 0.01 M (d–f) nutrient solution, respectively. Panel (c) shows the XRD patterns of the pristine Ag NWs (bottom curve) and the resulting ZnO NR-grown Ag NWs (upper curve).

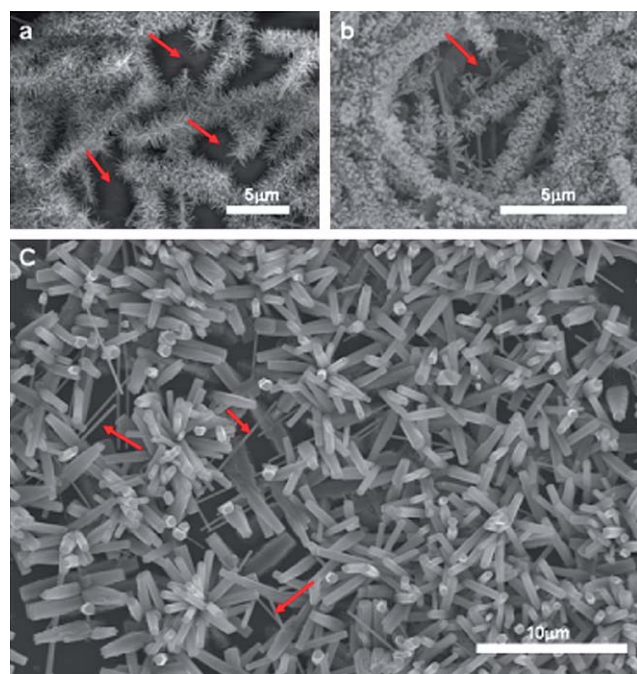


**Fig. 3** SEM images of the as-prepared ZnO NRs in the case of the substrate sparsely covered with the ZnO seed-coated Ag NWs (a and b) and the pristine Ag NWs (c): (a) 0.01 M  $\text{Zn}(\text{NO}_3)_2/\text{HMT}$ ; (b) and (c) 0.05 M  $\text{Zn}(\text{NO}_3)_2/\text{HMT}$ , respectively.

demonstrate that each branched NR actually consists of the primary ZnO NR and the secondary vertically grown shorter ZnO NRs on its side surfaces (Fig. 4e and f). Furthermore, these

shorter ZnO NRs have the same [001] growth direction as the backbone of ZnO NRs (Fig. 4f). This means the ZnO BNRs, which are covered densely by shorter NRs whose (001) facets are exposed at rod tips, are actually surrounded by active surface of (001) facets contributed by the numerous shorter NRs (Scheme 2). Hence, by means of the simple secondary growth method, the inert surface of ZnO has switched to an active surface with increased surface area as well as improved photoelectric activity (Scheme 2), which will be proved in photocatalytic measurements later. Furthermore, the Ag–ZnO heteroassemblies with the simple synthesis strategy can be extended as novel templates to synthesize other functional heterostructures, for example, Ag NW–CdS nanotube heteroassemblies, with promising applications (see Fig. S3†).

It is interesting that ZnO nanosheets (ZnO NSs) grown on Ag NWs with top/bottom faces as  $\pm(001)$  planes can be obtained when ZnO seed-coated Ag NWs are directly immersed in the same growth solution for ZnO BNRs (see S3 and Fig. S4†). The different structures of ZnO shorter NRs or ZnO NSs produced in the same citrate-contained solution result possibly from the different nucleation sites *i.e.* lateral facets of ZnO NRs and ZnO seeds. Comparably, ZnO NRs with exposed lateral (100) planes as nucleation sites favor more epitaxial growth, due to the defined structure match between specific crystal planes, such as the (0002) and (10 $\bar{1}$ 1) planes of ZnO.<sup>28,29</sup> This is one possibility responsible for the epitaxial growth of the shorter ZnO NRs on the side surface of the parent ZnO NRs. On the other hand, the presence of citrate ions plays the decisive role in the above formation of branched NRs. Namely, citrate ions preferentially adsorb to the (001) surfaces, which inhibits crystal growth along the [001] direction of the former primary ZnO nanorods.<sup>24</sup> It is

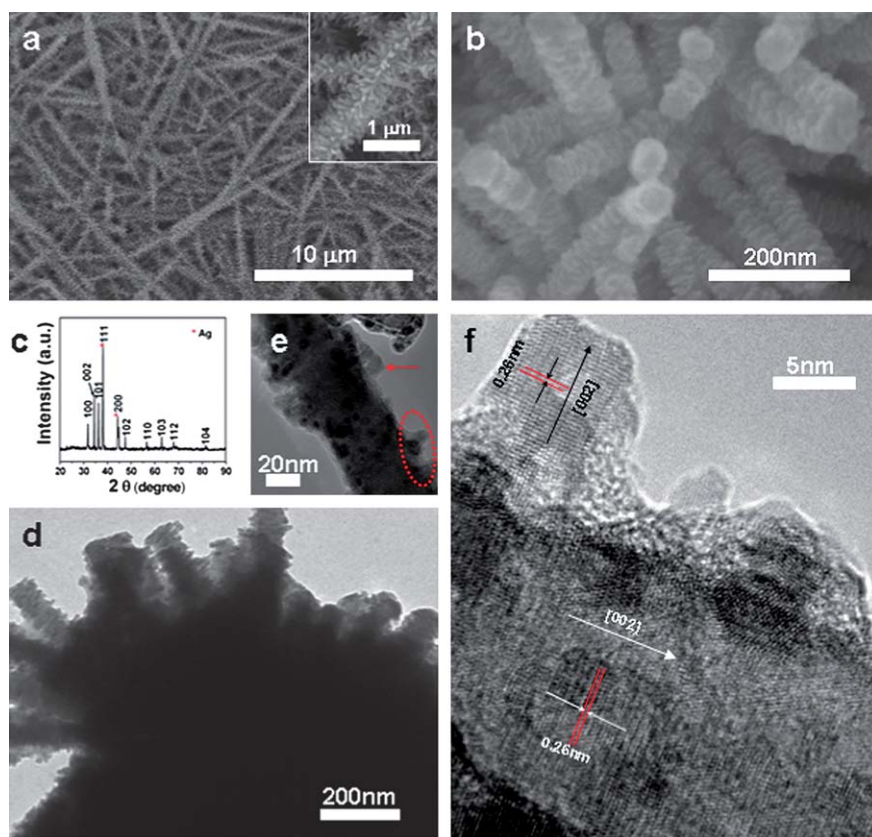
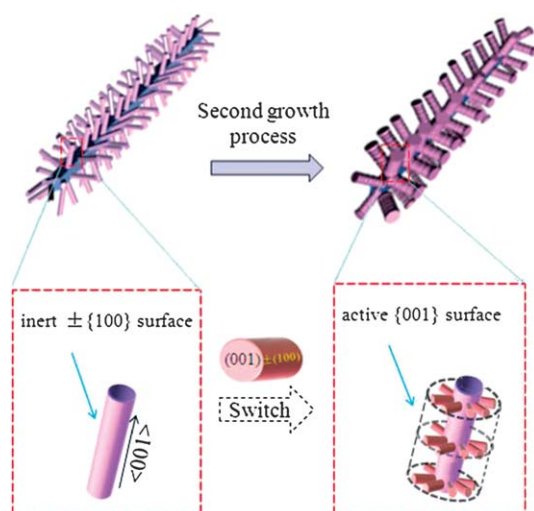


**Fig. 4** SEM (a and b), TEM (d), and HRTEM (e and f) images of the as-prepared Ag NW-ZnO BNR heteroassemblies. Panel (c) shows the corresponding XRD pattern. The circled part in (e) is further magnified in (f).



**Scheme 2** A schematic illustration of the surface property switch of Ag NW-based ZnO nanorod arrays from inert  $\{100\}$  planes to active  $\{001\}$  planes after the second growth process.

noted that in our case, the secondary growth occurs mainly on the lateral facets of ZnO NRs, different from the as-reported oriented nanocolumns (or nanoplates) selectively grown on the top (001) polar plane of ZnO NRs.<sup>24,28</sup> In both cases, citrate ions exist in the secondary growth solution and no ZnO seeds have been pre-adsorbed on the underlying ZnO NRs. Here it is not

clear what leads to the different secondary growth mode on ZnO NRs. We suppose the concentration of citrate ions and the incubation temperature may be involved. On the other hand, under the same conditions without citrate ions added to the fresh nutrient solution, new nucleation is not observed and the secondary growth just leads to the increase of the size and length of the primary ZnO NRs on Ag NWs. This fact indicates that under our conditions, the citrate ions, maybe like other structure-directing agents, promote the new site-specific heterogeneous nucleation and the sequential secondary growth.<sup>28</sup>

Herein, the photocatalytic performances of the Ag NW-based assemblies are evaluated by photodegradation of RhB in the aqueous solution, which is a typical organic azo-dye pollutant in the textile industry. For comparisons, pure ZnO NRs and NSs arrayed on coverslips have also been prepared by similar methods (S4, ESI†) and investigated by photocatalysis together. It is noted that all the samples are deposited on  $2 \times 2 \text{ cm}^2$  coverslips and immersed face-up in the solution of RhB under irradiation of a high pressure Hg lamp. The corresponding photocatalytic properties have been demonstrated in Fig. 5. Obviously, the degradation process approximately complies with the pseudo-first-order kinetics

$$\ln\left(\frac{C}{C_0}\right) = -kt$$

here,  $C_0$  and  $C$  are the initial concentration of RhB and the concentration of exposure time  $t$ , which correspond well to the

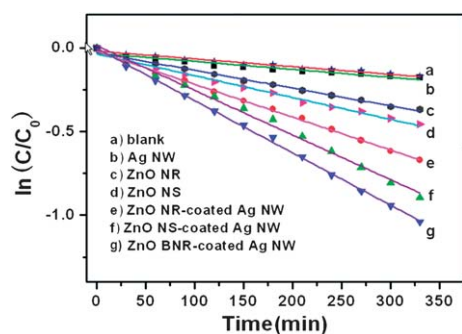
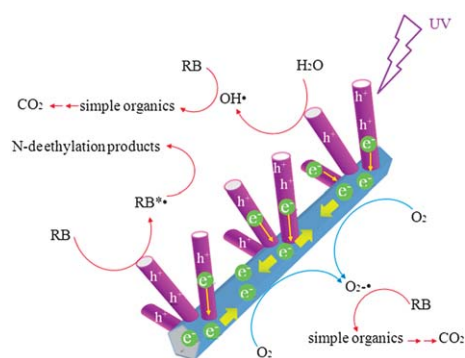


**Fig. 5** The photocatalytic properties of the as-prepared hierarchical nanostructures of Ag NW-based assemblies as well as the blank (without any catalyst added), the pure Ag NWs, ZnO NRs and ZnO NSs which were grown on the ZnO seed-coated substrates.

absorbance of RhB at 554 nm, respectively.  $k$  is the degradation constant. The photocatalytic efficiency estimated follows the order: Ag NWs–ZnO BNRs > Ag NWs–ZnO NSs > Ag NWs–ZnO NRs > ZnO NSs > ZnO NRs > Ag NWs > blank (*i.e.*, no catalyst added) (Fig. 5). The typical Ag NWs–ZnO BNR heterostructures demonstrated higher photocatalytic activity than other pure/hetero-nanostructured catalysts. Furthermore, compared with the common catalysts in the form of dispersed nanoparticles in the reaction media, our Ag NW-based nanostructures deposited on the substrates are more conveniently separated and recycled without any laborious centrifugation.

From the results of RhB photodegradation, some more conclusions and discussion can be given as follows: (i) self-degradation of RhB and the photocatalytic role of the pure Ag NWs upon UV irradiation are negligible, as shown in linear lines (a) and (b). (ii) Ag NW-based heteroassemblies display a greatly improved photocatalytic property compared with their pure counterparts. Since Ag NWs are inert to this photo-degradation reaction, obviously, the enhancement should be ascribed to the synergistic effect of Ag–ZnO heterojunctions and the hierarchical fluffy worm-like morphologies. It is reported that the Ag–ZnO heterostructures facilitate more effective separation of photoinduced electrons and holes and reduce the charge recombination significantly due to their equilibrium band structure.<sup>8–11</sup> Under UV irradiation, photoelectrons will transfer quickly from the surface of ZnO to Ag NWs, leaving a quantity of holes on the ZnO surface.<sup>9,30</sup> Especially, it is stressed here that 1D structured Ag NWs and ZnO NRs with high carrier transport property, serve as spatially extended catalyzing centers to provide direct and fast electron/hole transfer to their acceptors ( $H_2O$ ,  $O_2$ , RhB), which increase the chance of RhBs to be degraded, compared with commonly used isolated Ag–ZnO particles (Scheme 3). On the other hand, the hierarchical heteroassemblies with branched structures endow the catalysts with a larger specific surface area and more accessible active sites for improved light harvesting as well as enhanced diffusion and adsorption of RhB molecules. (iii) The photocatalytic properties of ZnO NSs and ZnO BNRs with exposed (001) plane are better than that of Zn NRs surrounded with (100) plane, regardless of Ag NW existence, which is ascribed to the higher activity of the (001) plane.<sup>27</sup> Accordingly, with all the above merits, the Ag NW–ZnO BNR heteroassemblies obtained the best



**Scheme 3** The speculated photocatalytic mechanism of fluffy worm-like Ag NW–ZnO NR heteroassemblies.

photocatalytic performance in the measurement. In fact, photocatalysis is a complicated process, which is associated with not only the structure-related physical properties such as crystal plane energy and charge separation, transportation and recombination of catalysts, but also structure-related catalytic processes regarding light harvesting and molecule diffusion kinetics and adsorption thermodynamics.

## 4. Conclusions

In summary, ZnO BNRs have been selectively assembled on the film of interwoven Ag NWs in a large area under different aqueous-solution conditions. Moreover, they exhibited high photocatalytic properties over the other homogeneous structures of ZnO NR arrays and ZnO NSs, or heteroassemblies of Ag NWs–ZnO NRs and Ag NWs–ZnO NSs. Such high performances arise from the synergistic effect of the special metal–heterojunctions and the hierarchical fluffy worm-like morphologies with exposed highly active (001) planes of ZnO and high specific surface area. Additionally, compared with traditional photocatalysts in the form of NPs, these hierarchical assemblies deposited on arbitrary substrates with high specific surface areas are easy to separate and recycle. Considering the high electrical conductivity and good resistance to corrosion, Ag NWs have been successfully used to construct transparent mesh electrodes instead of ITO.<sup>12,13,18</sup> Therefore, our diverse Ag NW-based nanostructures, when deposited on plastic or elastomeric substrates, also have great potentials as deformable solar cells,<sup>12,13,18</sup> electro-chemiluminescence sensors<sup>31</sup> and so on. These related investigations are under way. Furthermore, this simple versatile synthesis strategy can be extended to other hierarchical heterogeneous assemblies to obtain novel unprecedented multi-functions and properties.

## Acknowledgements

Financial support from the Natural Science Foundation of China (no. 20874072, 21074090, 21001082), Program for New Century Excellent Talents in University, Scientific Research Foundation for the Returned Overseas Chinese Scholars of State Education Ministry, Shanghai Pujiang Program (10PJ1410400), Visiting scholar fund of the Key Laboratory for Ultrafine Materials of Ministry of Education, East China University of

Science and Fundamental Research Funds for the Central Universities is gratefully acknowledged.

## References

- 1 S. E. Habas, P. D. Yang and T. J. Mokari, *J. Am. Chem. Soc.*, 2008, **130**, 3294.
- 2 F. R. Fan, Y. Ding, D. Y. Liu, Z. Q. Tian and Z. L. Wang, *J. Am. Chem. Soc.*, 2009, **131**, 12036.
- 3 L. Wu, B. G. Quan, Y. L. Liu, R. Song and Z. Y. Tang, *ACS Nano*, 2011, **5**, 2224.
- 4 J. Yang and J. Y. Ying, *Angew. Chem., Int. Ed.*, 2011, **50**, 4637.
- 5 J. S. Lee, E. V. Shevchenko and D. V. Talapin, *J. Am. Chem. Soc.*, 2008, **130**, 9673.
- 6 R. Costi, A. E. Saunders, E. Elmalem, A. Salant and U. Banin, *Nano Lett.*, 2008, **8**, 637.
- 7 C. Pacholski, A. Kornowski and H. Weller, *Angew. Chem., Int. Ed.*, 2004, **43**, 4774.
- 8 C. L. Ren, B. F. Yang, M. Wu, J. Xu, Z. P. Fu, Y. Lv, T. Guo, Y. X. Zhao and C. Q. Zhu, *J. Hazard. Mater.*, 2010, **182**, 123.
- 9 C. D. Gu, C. Cheng, H. Y. Huang, T. L. Wong, N. Wang and T. Y. Zhang, *Cryst. Growth Des.*, 2009, **9**, 3278.
- 10 M. J. Height, S. E. Pratsinis, O. Mekasuwandumrong and P. Praserthdam, *Appl. Catal., B*, 2006, **63**, 305.
- 11 C. Karunakaran, V. Rajeswari and P. Gomathisankar, *Solid State Sci.*, 2011, **13**, 923.
- 12 L. B. Hu, H. S. Kim, J. Y. Lee, P. Peumans and Y. Cui, *ACS Nano*, 2010, **4**, 2955.
- 13 C. Yang, H. W. Gu, W. Lin, M. M. Yuen, C. P. Wong, M. Y. Xiong and B. Gao, *Adv. Mater.*, 2011, **23**, 3052.
- 14 Y. G. Sun and Y. N. Xia, *Adv. Mater.*, 2002, **14**, 833.
- 15 A. Tao, F. Kim, C. Hess, J. Goldberger, R. R. He, Y. G. Sun, Y. N. Xia and P. D. Yang, *Nano Lett.*, 2003, **3**, 1229.
- 16 H. Y. Shi, B. Hu, X. C. Yu, R. L. Zhao, X. F. Ren, S. L. Liu, J. W. Liu, M. Feng, A. W. Xu and S. H. Yu, *Adv. Funct. Mater.*, 2010, **20**, 958.
- 17 Y. G. Sun, *Nanoscale*, 2010, **2**, 1626.
- 18 J. Lee, S. Connor, Y. Cui and P. Peumans, *Nano Lett.*, 2008, **8**, 689.
- 19 (a) L. Cheng and L. M. Qi, *Adv. Mater.*, 2010, **22**, 1494; (b) L. Schmidt-Mende and J. L. MacManus-Driscoll, *Mater. Today*, 2007, **10**, 40.
- 20 I. Gonzalez-Valls and M. Lira-Cantu, *Energy Environ. Sci.*, 2010, **3**, 789.
- 21 J. H. Yang, G. M. Liu, J. Lu, Y. F. Qiu and S. H. Yang, *Appl. Phys. Lett.*, 2007, **90**, 103109.
- 22 Z. L. Wang, *ACS Nano*, 2008, **2**, 1987.
- 23 Y. Gao, P. Jiang, D. F. Liu, H. J. Yuan, X. Q. Yan, Z. P. Zhou, J. X. Wang, L. Song, L. F. Liu, W. Y. Zhou, G. Wang, C. Y. Wang and S. S. Xie, *Chem. Phys. Lett.*, 2003, **380**, 146.
- 24 Z. R. Tian, J. A. Voigt, J. Liu, B. Mckenzie, M. J. Mcdermott, M. A. Rodriguez, H. Konishi and H. F. Xu, *Nat. Mater.*, 2003, **2**, 821.
- 25 L. E. Greene, M. Law, J. Goldberger, F. Kim, J. C. Johnson, Y. F. Zhang, R. J. Saykally and P. D. Yang, *Angew. Chem., Int. Ed.*, 2003, **42**, 3031.
- 26 X. L. Cao, H. B. Zeng, M. Wang, X. J. Xu, M. Fang, S. L. Ji and L. D. Zhang, *J. Phys. Chem. C*, 2008, **112**, 5267.
- 27 E. Jang, J. Won, S. Hwang and J. Choy, *Adv. Mater.*, 2006, **18**, 3309.
- 28 T. R. Zhang, W. J. Dong, M. Keeter-Brewer, S. Konar, R. N. Njabon and Z. R. Tian, *J. Am. Chem. Soc.*, 2006, **128**, 10960.
- 29 F. H. Zhao, J. G. Zheng, X. F. Yang, X. Y. Li, J. Wang, F. L. Zhao, K. S. Wong, C. L. Liang and M. M. Wu, *Nanoscale*, 2010, **2**, 1674.
- 30 Y. H. Zheng, L. R. Zheng, Y. Y. Zhan, X. Y. Lin, Q. Zheng and K. M. Wei, *Inorg. Chem.*, 2007, **46**, 6980.
- 31 C. Z. Wang, Y. F. E, L. Z. Fan, S. H. Yang and Y. L. Li, *J. Mater. Chem.*, 2009, **19**, 3841.
- 32 C. Pacholski, A. Kornowski and H. Weller, *Angew. Chem., Int. Ed.*, 2002, **41**, 1188.